NeuroImage: Clinical 29 (2021) 102539

Contents lists available at ScienceDirect

NeuroImage: Clinical

journal homepage: www.elsevier.com/locate/ynicl

Stroke core revealed by tissue scattering using spatial frequency domain imaging

Smrithi Sunil [a,*], Sefik Evren Erdener [a,b], Xiaojun Cheng [a], Sreekanth Kura [a], Jianbo Tang [a], John Jiang [a], Kavon Karrobi [a], Kıvılcım Kılıç [a], Darren Roblyer [a,c], David A. Boas [a,c]

[a] Department of Biomedical Engineering, Boston University, Boston, MA 02215, USA
[b] Institute of Neurological Sciences and Psychiatry, Hacettepe University, Ankara, Turkey
[c] Department of Electrical and Computer Engineering, Boston University, Boston, MA 02215, USA

ARTICLE INFO

Keywords:
Stroke
Spatial frequency domain imaging
Optical scattering
Optical coherence tomography
TTC staining

ABSTRACT

Ischemic stroke leads to a reduction or complete loss of blood supply causing injury to brain tissue, which ultimately leads to behavioral impairment. Optical techniques are widely used to study the structural and functional changes that result as a consequence of ischemic stroke both in the acute and chronic phases of stroke recovery. It is currently a challenge to accurately estimate the spatial extent of the infarct without the use of histological parameters however, and in order to follow recovery mechanisms longitudinally at the mesoscopic scale it is essential to know the spatial extent of the stroke core. In this paper we first establish optical coherence tomography (OCT) as a reliable indicator of the stroke core by analyzing signal attenuation and spatially correlating it with the infarct, determined by staining with triphenyl-tetrazolium chloride (TTC). We then introduce spatial frequency domain imaging (SFDI) as a mesoscopic optical technique that can be used to accurately measure the infarct spatial extent by exploiting changes in optical scattering that occur as a consequence of ischemic stroke. Additionally, we follow the progression of ischemia through the acute and sub-acute phases of stroke recovery using both OCT and SFDI and show a consistently high spatial overlap in estimating infarct location. The use of SFDI in assessing infarct location will allow longitudinal studies targeted at following functional recovery mechanisms on a mesoscopic level without having to sacrifice the mouse acutely.

1. Introduction

In ischemic stroke, a reduction or complete loss in blood supply to a region of the brain results in a cascade of events over a varied temporal scale of minutes (hyperacute) and hours (acute), to days and ultimately weeks (chronic) (Lo et al., 2003; Moskowitz et al., 2010; Murphy and Corbett, 2009). The region directly supplied by the occluded vessel sees the largest reduction in blood flow (20% of normal flow) and undergoes cellular death within minutes of an occlusion. This area of metabolically dead tissue is referred to as the core of the stroke and the region surrounding the core contains hypo-perfused tissue that is damaged but not yet dead (Lo, 2008). This peripheral area that represents salvageable tissue is called the penumbra in the acute phase or the peri-infarct in the chronic phase. When properly managed with timely interventions, the penumbra can be saved before the core expands into it (Chalela et al., 2004; Chatterjee, 2012; Parsons et al., 2002). In the chronic phase, the peri-infarct undergoes significant spontaneous reorganization and restoration that results in functional and behavioral recovery (Cassidy and Cramer, 2017; Cramer, 2008a).

Preclinical animal models provide a great tool to study the structural and functional consequences of ischemic stroke (Bacigaluppi et al., 2010; Carmichael, 2005; Traystman, 2003) and are used extensively to enhance our understanding of stroke recovery mechanisms (Brown et al., 2009, 2007; Schrandt et al., 2015; Winship and Murphy, 2008). This understanding through experimental research goes hand-in-hand with the advancements seen in optical imaging techniques. Laser speckle contrast imaging (LSCI) allows visualization of changes to relative cerebral blood flow (CBF) before and after stroke over a large field of view with relatively high spatial (10–100 μm) and temporal resolution (10–100 frames/sec) (Ayata et al., 2004; Boas and Dunn, 2010; Dunn et al., 2001). In the acute phase following occlusion, LSCI can be used to closely monitor tissue perfusion in the core and penumbra, as well as evaluate the effect of treatment on tissue reperfusion and recovery. Optical coherence tomography (OCT) has been used to obtain

* Corresponding author.
E-mail address: ssunil@bu.edu (S. Sunil).

https://doi.org/10.1016/j.nicl.2020.102539
Received 18 July 2020; Received in revised form 14 December 2020; Accepted 15 December 2020
Available online 20 December 2020

absolute blood flow measures over several millimeters with micron-level resolution (Tang et al., 2018, 2017; Wang et al., 2017) and two-photon microscopy is capable of imaging cellular-level information down to hundreds of microns below the brain surface (Helmchen and Denk, 2005). Longitudinal stroke recovery occurs both spontaneously and can be enhanced through rehabilitation. Functional neuroimaging methods are valuable for monitoring these recovery processes (Blicher et al., 2012; Johansen-berg, 2007; Johansen-Berg et al., 2002; Lake et al., 2016).

A number of studies have been performed to follow neuronal and vascular recovery mechanisms longitudinally in the peri-infarct (Brown et al., 2007; Schrandt et al., 2015). These studies typically rely on CBF as a metric to define either the stroke core or the peri-infarct region. While CBF has been validated as a reliable metric in determining the extent of tissue damage, the CBF cut-off values for the core and peri-infarct vary across different studies (Dunn, 2012; Parthasarathy et al., 2010; Strong et al., 2006). In addition, CBF obtained from LSCI is a relative measure that can depend on the instrumentation and experimental parameters. Histological staining of brain tissue with triphenyl-tetrazolium chloride (TTC) has been well established as a gold-standard to identify the stroke core as TTC can differentiate between metabolically active and inactive tissue (Türeyen et al., 2004). However, the drawback with TTC staining is that it needs to be performed within 72 h of the stroke in order to be a reliable measure of the infarct and requires the animal to be sacrificed, thereby not allowing valuable longitudinal studies.

Traditionally, the stroke core has been evaluated longitudinally with diffusion weighted imaging (DWI) which is a type of magnetic resonance imaging that measures the apparent diffusion coefficient (ADC) of water within the brain tissue (Meng et al., 2004; Neumann-haefelin et al., 1999). Perfusion deficits, which lead to metabolic energy failure, result in cellular swelling in the early hours after ischemic stroke (Liang et al., 2007; Somjen, 2001). Cellular swelling results in a decrease in ADC, which is measured as an increase in the DWI signal. Although DWI is a widely accepted method, it is hard to implement due to high cost and space constraints related to MRI instrumentation. It is expected that cellular and intracellular organelle swelling also changes the optical scattering coefficient within the brain tissue, as has been observed with OCT (Choi et al., 2019; Srinivasan et al., 2013). Tissue scattering or light attenuation obtained from microscopy techniques, such as OCT, are optical analogs to DWI and are expected to be reliable metrics of the stroke core that can help guide longitudinal monitoring of functional recovery following stroke, as suggested in recent publications (Choi et al., 2019; Srinivasan et al., 2013).

OCT typically captures micrometer-resolution three-dimensional images across a few millimeter (1–3 mm) fields of view from within optically scattering samples such as the brain. For monitoring the stroke core in animal models, it is advantageous to compliment the OCT measures with mesoscopic resolution over larger fields of view (6–10 mm) that cover the entire mouse cortex. Spatial frequency domain imaging (SFDI) is a wide-field diffuse optical reflectance-based technique that can quantify sample absorption (μ_a) and reduced scattering (μ_s') coefficients (Cuccia et al., 2009; Gioux et al., 2019). While SFDI has been used to study the hemodynamic response during ischemic stroke (Abookasis et al., 2009), it has not been used in the context of longitudinally mapping the stroke core. This approach may be useful for combining stroke lesion identification with other wide-field imaging such as calcium signals or intrinsic optical signal imaging. In this paper we present SFDI as an optical technique to accurately measure the spatial extent of the stroke core. We follow the optical evolution of the stroke core before and after the onset of stroke and at various time points until 72 h post-stroke. We first validate that OCT signal attenuation can reliably predict the stroke core by comparing to TTC staining. SFDI scattering is then validated alongside OCT signal attenuation following which SFDI is validated against TTC staining.

2. Methods

2.1. Instrumentation

A schematic of our imaging setup used for producing a stroke with photothrombosis and then monitoring it with spatial frequency domain imaging is shown in Fig. 1. Our combined laser speckle contrast imaging (LSCI) and photothrombosis setup for optimized induction of photothrombotic stroke has been described in detail previously (Sunil et al., 2020). In order to induce an occlusion in a distal pial branch of the middle cerebral artery (MCA) and simultaneously monitor changes to cerebral blood flow (CBF), the photothrombosis setup was coupled together with the LSCI system. Briefly, LSCI is used to image CBF by illuminating the surface of the brain with a 785 nm laser diode (LP785-SAV50, Thorlabs) and imaging the back scattered light using a CMOS camera (Basler acA2040-90um NIR). A 785 nm band pass filter, with a bandwidth of 10 nm, along the detection path was used to spectrally restrict the light. Additionally, in order to minimize specular reflections and optimize the speckle size a linear polarizer and iris were placed along the imaging path respectively. The pupil diameter of the iris was adjusted such that the speckle to pixel size ratio was 3.2 as calculated from the spatial cross-correlation of the speckle pattern obtained from a static scattering sample. Speckle images were acquired with a 5 ms exposure time at 40 frames per second. To perform photothrombosis via photoactivation of a photosensitive dye, Rose Bengal, the system contains a 520 nm laser diode in an epi-illumination configuration. The laser spot size was designed to obtain a lateral resolution of 6 μm in diameter with an axial point spread function of 104 μm. A beam splitter along the imaging path allows visualization of the laser spot on the scientific CMOS camera (Hamamatsu ORCA-Flash4.0V3). A 470 nm LED (not shown in the schematic) was used to illuminate the surface vasculature in order to position the laser spot on the target pial vessel. A 640 nm dichroic beam-splitter was used to split the near-infrared and visible light and a 650 nm short pass filter was used to prevent bleed through from the 785 nm laser diode used for LSCI. The imaging setup includes a 2X objective for a field of view of 5.6 mm × 5.6 mm for the CMOS (LSCI camera) and 6.5 mm × 6.5 mm for the sCMOS.

Instrumentation for spatial frequency domain imaging (SFDI) has been added to this imaging setup to allow estimation of tissue optical properties including the absorption (μ_a) and reduced scattering coefficients (μ_s') (Applegate et al., 2020). A 530 nm LED was used for SFDI so that the absorption images would be representative of total hemoglobin concentration without confounding impacts of hemoglobin oxygenation. A digital micromirror device (DMD) (LC4500, Keynote Photonics) along the illumination path is used to spatially modulate the light at the desired frequencies. An achromatic lens is placed after the DMD along the illumination path to magnify the image from the DMD onto the sample. Additionally, a polarizer is placed along the illumination and imaging paths in order to cross polarize the light and reduce specular reflections. A mirror along the illumination path is placed after the polarizer to direct and center the light beam on the mouse brain. The reflected light is captured with the sCMOS camera.

2.2. Surgical procedure

All animal procedures were approved by the Boston University Institutional Animal Care and Use Committee and were conducted following the Guide for the Care and Use of Laboratory Animals. All mice used in this study were adult wildtype C57Bl6 at approximately 15 weeks old. A total of 7 mice were used in the study, 4 mice were sacrificed at 24 h after stroke and 3 mice were sacrificed at 72 h after stroke for histological analysis.

Our surgical procedure has been described previously (Sunil et al., 2020). Briefly, 4 h prior to the start of surgery, dexamethasone was administered intraperitoneally in order to minimize cerebral edema during and after surgery. Isoflurane was used to anesthetize the mice

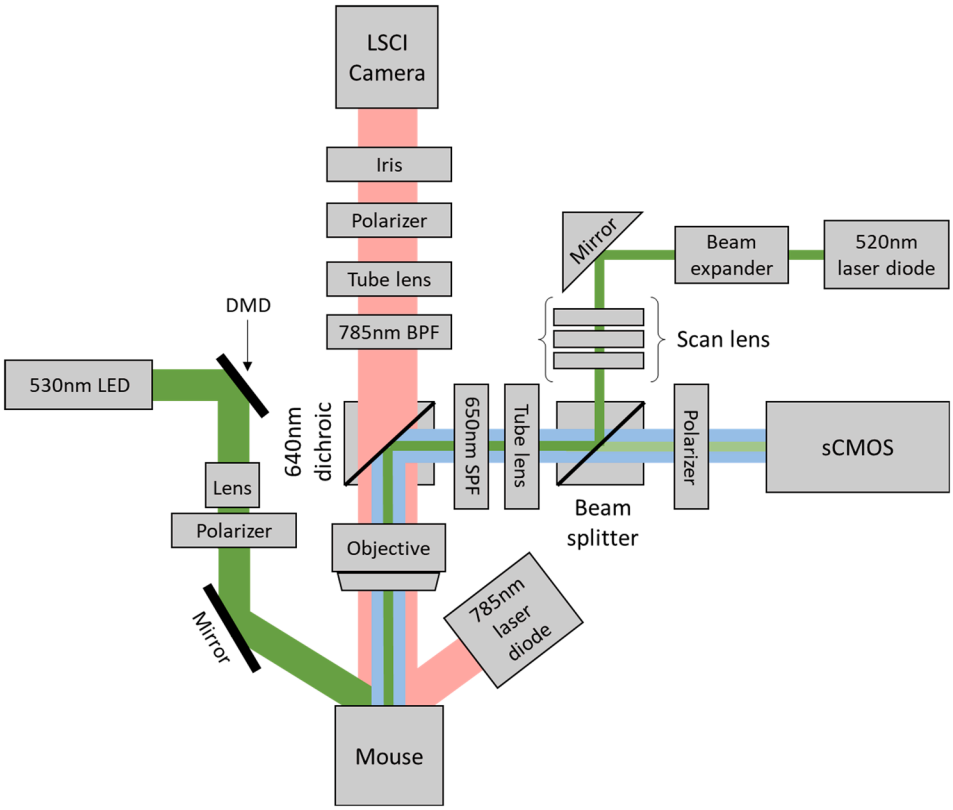

Fig. 1. Schematic of the imaging setup with combined photothrombosis, laser speckle contrast imaging, and spatial frequency domain imaging.

(3% at induction and 1–1.5% for maintenance with 1 L/min oxygen), while body temperature was maintained at 37 °C with a homeothermic blanket. Respiratory rate and toe pinch were used to monitor the depth of anesthesia throughout the surgical procedure. After incision of the scalp, a craniotomy was performed on one hemisphere of the brain in order to remove the skull. A half-skull-shaped curved glass (Kim et al., 2016) (modified from Crystal Skull, LabMaker, Germany) was used to cover the surface of the brain and then sealed with dental acrylic. To allow head-fixation of the mice under the imaging system, an aluminum head post was attached to the intact skull of the other hemisphere. After a 10 day recovery period from surgery, mice were trained to remain head-fixed for up to 1 h for approximately 7 days. All experiments are done in awake head-fixed mice.

2.3. Focal cerebral ischemia

Optimized photothrombosis was performed as described in our previous paper (Sunil et al., 2020). A modified version of photothrombosis previously described by Watson et al. (1985), Watson et al. (1985) was used to perform an occlusion of a distal pial branch of the middle cerebral artery (MCA). The 520 nm laser diode was tuned to a post-objective focal power of 0.6 mW prior to the start of photothrombosis. The surface vasculature was visualized under the 470 nm LED and the mouse was positioned so that the laser spot is directly over the target vessel. Ten minutes of baseline CBF was obtained following which the mouse was lightly anesthetized for retroorbital injection of Rose Bengal (100 μl, 15 mg/ml in saline). The active use of isoflurane is limited to under one minute, which includes induction and injection, after which the mouse is immediately taken off isoflurane and allowed to recover. Recovery of the mouse was determined as a return to baseline CBF and exhibiting natural behavior such as whisking. Our optimized photothrombosis protocol uses real-time laser speckle contrast feedback to guide the duration of illumination in order to minimize unwanted photodamage to the surrounding vasculature as a consequence of laser illumination. The 520 nm laser was turned on until the target vessel was occluded, as indicated by a disappearance of the branch in real-time LSCI, and then decreased to half the power for two minutes. Real-time spatial laser speckle contrast was calculated from the raw images captured using software from The Functional Optical Imaging Laboratory at The University of Texas at Austin (Ponticorvo and Dunn, 2010). The mouse was monitored for 1 h under the LSCI setup and if the branch reperfused during this time, the laser was turned on again until subsequent occlusion. Additionally, as previously described, two collateral branches were also targeted in order to obtain a stable infarct.

2.4. Optical coherence tomography

In order to validate the scattering maps obtained from SFDI we used optical coherence tomography (OCT). OCT signal attenuation has been used and validated previously as a technique to obtain the spatial extent of the stroke core (Choi et al., 2019; Srinivasan et al., 2013). OCT angiograms of the vasculature were obtained at pre-stroke, 1 h, 2 h, 4 h, 24 h, and 72 h after photothrombosis. A spectral domain OCT system (1310 nm center wavelength, bandwidth 170 nm, Thorlabs) was used for obtaining angiograms as previously described (Erdener et al., 2017). A 5X objective (Mitutoyo) was used to obtain a field of view of 2.5 mm × 5 mm. The region was scanned with 500 × 1000 pixels to obtain a pixel size of 5 × 5 μm^2. OCT angiograms were obtained using a repeated complex OCT B-scan signal. Each OCT image was repeated 5 times to obtain an average of 5 angiograms. The average of the raw signal was processed offline using a custom MATLAB code to extract the OCT signal attenuation. The signal intensity was calculated as the log of the average of the two repeated B-scans. The signal was spatially down-sampled in the XY-direction to minimize speckle noise by taking an average of pixels in the nearest 4x4 neighborhood. The OCT attenuation, defined as the slope of signal decay with respect to depth, was obtained by performing a first order polynomial fit to each pixel in the XY-direction. A 450 μm region in depth was selected, starting at approximately a 100 μm

below the glass, to perform the fit. Fig. 2 shows an outline of OCT analysis where Fig. 2(A) shows an OCT angiogram. Fig. 2(B) shows an XZ profile of the red line indicated in the left angiogram and the slope of signal decay from two points, one within the stroke (blue) and one outside the stroke (green). Fig. 2(C) shows OCT attenuation at each XY pixel where the darker pixels have a larger slope due to faster signal decay apparently depicting the stroke core.

2.5. Spatial frequency domain imaging

SFDI uses spatially varying sinusoidal patterns, which are projected onto a sample surface, and the reflected light is detected with a camera. The spatial modulation transfer function (sMTF), which contains optical property information, is obtained through a demodulation and calibration procedure performed on the reflected light. The sMTF is then calibrated with a silicone phantom to obtain the diffuse reflectance, which is then compared to the results obtained from Monte Carlo simulations of photon transport to determine absorption and reduced scattering. The instrumentation for SFDI is previously described in section 2.1 and was adapted from Applegate et al. (2020) (Applegate et al., 2020). A schematic of just the SFDI setup is shown in Fig. 3(A). Optical properties of the brain were obtained at pre-stroke, 1 h, 2 h, 4 h, 24 h, and 72 h after photothrombosis. The DMD in the illumination path spatially modulates the light at six spatial frequencies (0, 0.05, 0.1, 0.2, 0.4, 0.5 mm^{-1}) and each sinusoidal pattern is projected at three phases (0, 120, and 240 deg). The reflected light is captured with a sCMOS camera with a FOV of 6.5 mm × 6.5 mm and is synchronized with the mirror display and LED. Total acquisition time for 6 frequencies, at 3 phases, repeated 5 times is ~5 min or ~3 s/frame. In addition to imaging the awake mice, a silicone phantom with known optical properties is imaged with the same protocol to calibrate for system errors. The images obtained are processed offline using MATLAB following previously established protocols (Cuccia et al., 2009; Lin et al., 2013) to obtain a pixel-by-pixel map of the tissue optical properties. Demodulated intensity at each spatial frequency were calculated using:

$$M_{AC}(x_i,f_x) = \frac{2^{1/2}}{3}\left[(I_1 - I_2)^2 + (I_2 - I_3)^2 + (I_1 - I_3)^2\right]^{1/2}$$

where M_{AC} is the demodulated AC component and I_1, I_2, and I_3 are the reflected intensity images at the three phases for each spatial frequency. M_{AC} images were then calibrated to the reference phantom to obtain the diffuse reflectance. Measurements were analyzed using a lookup table (LUT) from Monte Carlo simulations (Boas et al., 2002), where the reflectance patterns are recorded for various values of μ_a and μ_s' with a point source as an input. The simulated spatial frequency dependent reflectance can be obtained by convolving the incident sinusoidal source pattern with the reflectance pattern obtained from the point source. We have assumed the anisotropy factor g = 0.9. A two frequency LUT was generated from the simulation results for spatial frequencies of 0 mm^{-1} and 0.4 mm^{-1}. While we obtained data for a range of spatial frequencies, only two spatial frequencies were used to generate the LUT and analyze the results. The spatial frequency used for analysis was chosen based on the orthogonality of the LUT, minimal coupling between μ_a and μ_s' in the LUT, and where most of the diffuse reflectance data points from the sample fell within the range of the LUT (Tabassum et al., 2016). This corresponded to the LUT of spatial frequencies 0 mm^{-1} and 0.4 mm^{-1}. Fig. 3(B) shows a flowchart of the SFDI data processing method. The top panel shows raw intensity images with planar (left) and sinusoidal (right) spatial patterns. The middle panel shows the diffuse reflectance images after AC demodulation of the three phases for each frequency and the bottom panel shows the absorption and reduced scattering coefficients obtained from the Monte Carlo LUT. Some cross-talk is observed in the extracted absorption and scattering images as seen by a decreased μ_a in the large blood vessels, which we expect to have higher absorption. The data points corresponding to the large vessels fall outside the range of the LUT, where there is coupling between μ_a and μ_s', therefore not allowing accurate estimation of the optical properties. Fig. 3(C) shows a visualization of the LUT and data points. The data points that fall outside the LUT are plotted in red along with their corresponding spatial location on the μ_s' image to more clearly indicate the points in the image for which we do not trust the estimated optical properties. We are primarily interested in changes to scattering within the parenchyma following stroke, which we can see falls within the LUT as shown by the green points in Fig. 3(C). Fig. 3(D) shows the reduced scattering coefficient in mm^{-1} before stroke and at three time points after stroke in the top panel. The bottom panel shows the percent change in reduced scattering coefficient compared to pre-stroke, where the stroke core is clearly highlighted due to increased scattering.

2.6. Histological analysis

We performed histological staining with triphenyl-tetrazolium chloride (TTC) to assess the stroke core at 24 h in 4 mice and 72 h in 3 mice. TTC has been well established as a technique for identifying infarcted tissue due to stroke by differentiating between metabolically

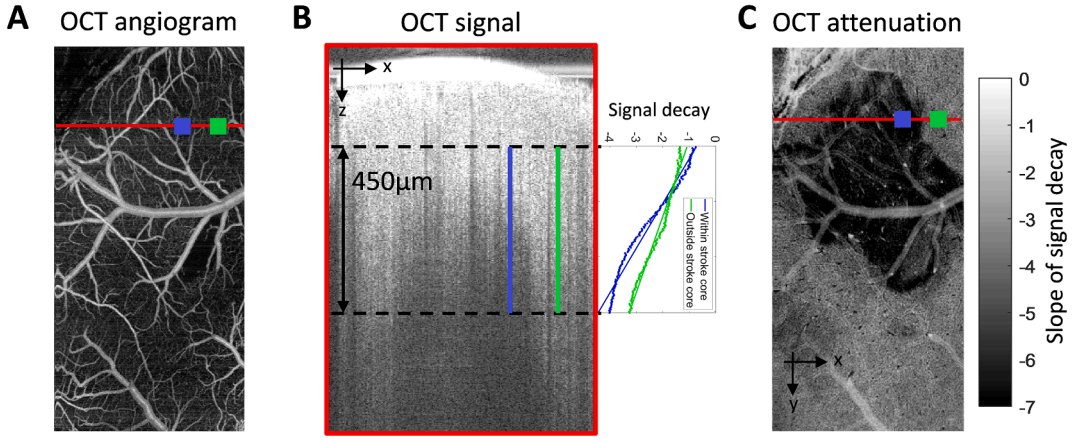

Fig. 2. (A) Example XY profile of an OCT angiogram from which a signal attenuation map is derived. (B) Left: XZ profile of a single line scan (red line in left panel) with 450 µm segment used to obtain signal attenuation. Right: OCT signal decay vs depth taken from two regions of interest, blue region lies within the stroke core and green region lies outside the stroke core. (C) XY map of OCT attenuation at 2 h after stroke. (For interpretation of the references to colour in this figure legend, the reader is referred to the web version of this article.)

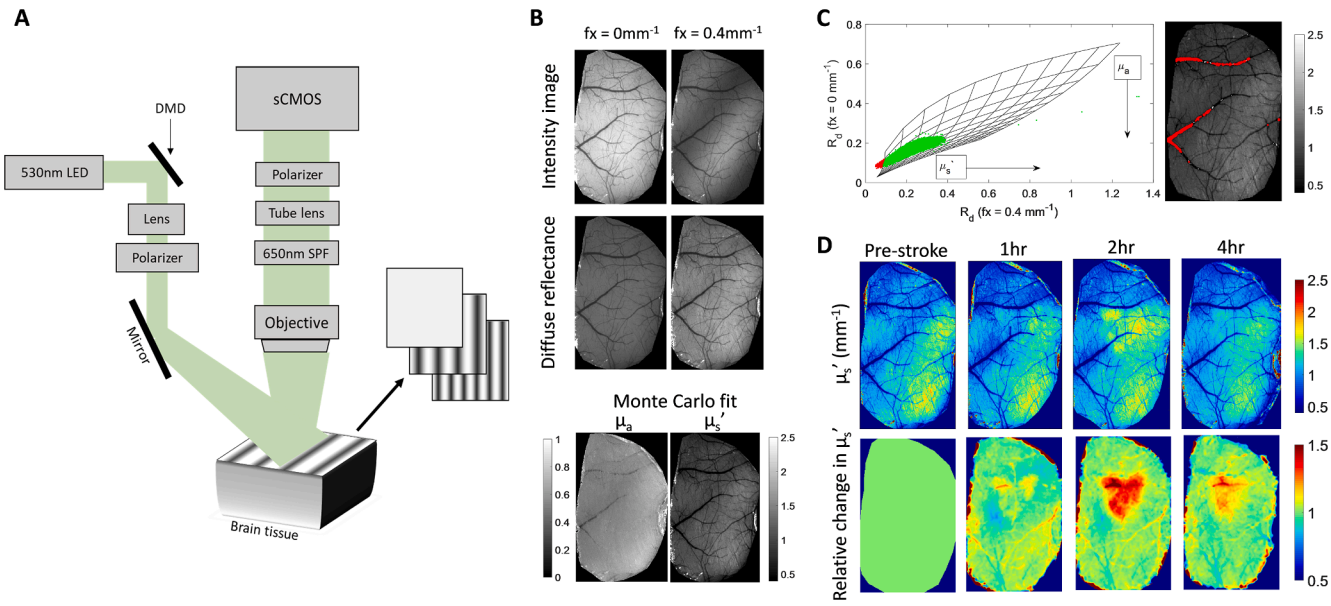

Fig. 3. (A) Imaging schematic of the spatial frequency domain imaging (SFDI) setup. (B) SFDI data processing flowchart: Intensity image at two frequencies (three phase images per frequency) are demodulated and calibrated with reference phantom images (diffuse reflectance) and then fit to a lookup table generated from Monte Carlo simulations to obtain μ_a and μ_s'. (C) Top row: Reduced scattering coefficient before and after photothrombosis, bottom row: percent change from baseline reduced scattering coefficient after photothrombosis.

active and inactive tissue (Türeyen et al., 2004). After the final imaging time point mice were deeply anesthetized with isoflurane, decapitated, and whole brain extracted for TTC staining. The intact brain was incubated at 37 °C for 30 min in 2% TTC in phosphate-buffered saline. Images were acquired immediately after staining under a surgical microscope.

2.7. Data analysis

All data were analyzed offline using custom MATLAB codes. First, the OCT and SFDI data were analyzed individually as described in the above sections. Then, SFDI scattering and OCT attenuation image from all time points of each animal were registered to the pre-stroke SFDI scattering image of the same animal. Once registered, the percent change in SFDI scattering and OCT signal attenuation were calculated from their respective pre-stroke values. In order to validate the spatial overlap between the stroke core as determined by SFDI and OCT we used the Dice coefficient, which is a statistic metric used to determine the similarity of two samples (Brendel et al., 2017; Wright et al., 2017; Zou et al., 2004). To calculate the overlap, a stroke core outline was semi-automatically drawn using built in MATLAB contour function, active-contour, for corresponding SFDI and OCT percent change images. The active contours technique is an iterative region-growing image segmentation algorithm that uses initial curves that are user specified after which the algorithm evolves the curves towards the object boundary. Each image had a user defined curve positioned within the core region. Each contour image was then converted into a binary image and the Dice coefficient built in function was used to assess the similarity between the two binary images. A total of 7 animals were used to calculate overlap between SFDI and OCT at all time points except 72 h, where 3 animals were used. In addition to estimating the spatial overlap with OCT, SFDI scattering was also validated with TTC staining using the same Dice coefficient procedure. Here, 5 animals were used (n = 2 at 24 h and n = 3 at 72 h) as 2 of the 4 animals sacrificed at 24 h did not show any distinct TTC abnormality. The green channel from the TTC image was used to register vascular landmarks from TTC with SFDI before performing similarity analysis. Quantitative results are expressed as mean and standard deviations.

3. Results

3.1. Increased OCT signal attenuation in a mouse photothrombosis stroke model is a reliable predictor of the stroke core

Prior studies have shown that OCT signal attenuation increases in the area of focal cerebral ischemia (Choi et al., 2019; Srinivasan et al., 2013). They have also shown the spatial expansion of signal attenuation as ischemia progressed over time and suggested that the infarcted tissue may be identified with these optical signals. However, OCT signal attenuation has not been statistically compared against the gold standard TTC stain for infarcted tissue. Here, we used the OCT XY-attenuation map with the co-registered TTC map to determine spatial overlap. Fig. 4(A) shows the spatial OCT attenuation map expressed as a slope of signal decay in the left panel. The right panel shows the percent change in OCT signal compared to the pre-stroke signal. Fig. 4(B) shows the TTC stain and the black outline corresponds to the cranial window location. The TTC image at the corresponding time point was co-registered to the OCT image and the dice coefficient was used to estimate overlap. There was a strong overlap between OCT and TTC with a similarity mean and standard deviation of 0.73 ± 0.13. Fig. 4(C) shows the similarity coefficient for individual animals (n = 5: n = 2 at 24 h, n = 3 at 72 h). Animals that did not show any apparent tissue infarct at 24 h were excluded from the analysis (n = 2).

3.2. Reduced scattering coefficient obtained from SFDI reliably predicts increased signal attenuation seen with OCT following stroke

While OCT provides microscopic information over millimeter fields of view in the brain, for monitoring the stroke core in animal models, it is advantageous to compliment the OCT measures with mesoscopic resolution over larger fields of view. This approach is useful when lesion identification is combined with other modalities such as calcium imaging or intrinsic optical signal imaging for neural and vascular dynamics respectively. Spatial frequency domain imaging (SFDI) is a wide-field diffuse optical technique that can separate sample absorption (μ_a) and reduced scattering (μ_s') coefficients. Cellular swelling in the acute time points following stroke has been well established and this swelling leads to an increase in optical scattering (Wilson et al., 2005; Yao et al., 2005).

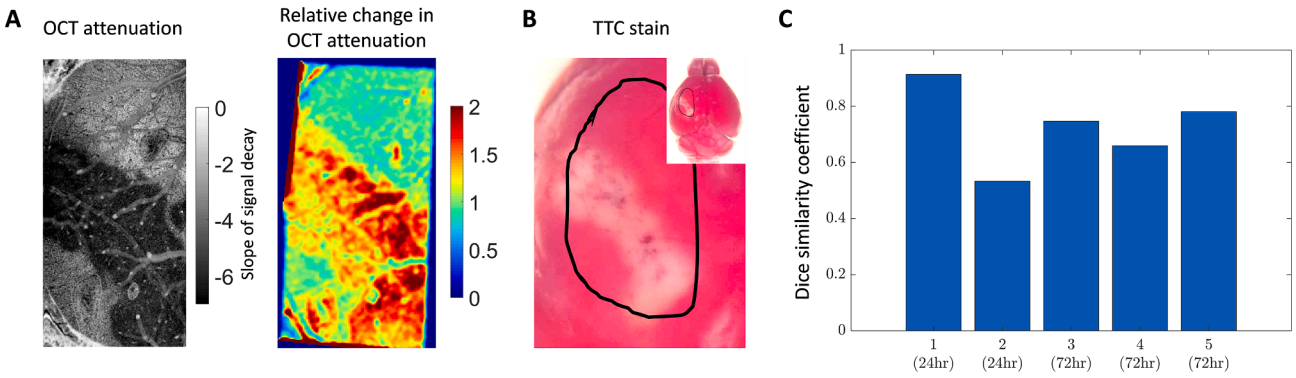

Fig. 4. Spatial overlap of OCT attenuation and TTC staining. (A) Left: OCT attenuation map at 72 h shown as the slope of signal decay, right: percent change in OCT attenuation at 72 h compared to pre-stroke. (B) TTC stain at 72 h after stroke, black outline indicates cranial window location. (C) Spatial overlap shown by Dice similarity coefficient for five mice.

Therefore, SFDI is potentially a great tool to longitudinally monitor the spatial progression of ischemia.

In order to validate SFDI as a technique that reliably predicts the stroke core, we can first verify that the reduced scattering coefficient obtained from SFDI spatially overlaps with OCT signal attenuation. Fig. 5 shows an example mouse with side-by-side comparison of SFDI and OCT. 5(A) shows the percent change in reduced scattering coefficient from SFDI (top row) and the percent change in co-registered OCT attenuation (bottom row) at various time points in the acute and subacute phases of stroke recovery. Qualitatively we observe good spatial overlap between the regions that show changes from pre-stroke at all the time points imaged after stroke. Fig. 5(B) shows the corresponding TTC stain at 72 h after stroke.

Quantitative analysis of spatial overlap also shows high similarity between OCT signal attenuation change and SFDI scattering change at all the time points after stroke except at 24 h. Fig. 6 shows the workflow and analysis for quantifying the Dice similarity coefficient. Fig. 6(A) shows an example SFDI and OCT percent change image, which is low-pass filtered, using a 2-D Gaussian filter with a standard deviation of 2, and automatically contoured by selecting a representative region of the stroke core. Fig. 6(B) shows the low-pass filtered and contoured image of the same example. The contours are then converted to a binary image and assessed for similarity. Fig. 6(C) shows the mean Dice similarity coefficient and standard deviation for all mice (n = 7 for the first 24 h and n = 3 for 72 h). All time points, except 24 h, show a larger than 70% overlap between SFDI scattering and OCT attenuation changes.

3.3. Scattering increase as determined from SFDI following photothrombotic stroke is a reliable predictor of the stroke core

Similar to validating OCT attenuation against TTC staining we validated SFDI with TTC staining as well in order to reveal the true stroke core. As described in section 3.1, we co-registered the TTC image with the SFDI percent change image at the corresponding time points and performed the similarity analysis (Fig. 7). Fig. 7(A) shows an example SFDI percent change image (left panel) that has been low-pass filtered and core outlined (right panel), and Fig. 7(B) shows the corresponding TTC image. The dice similarity coefficient for five animals is shown in Fig. 7(C). The mean spatial overlap was 0.74 with a standard deviation of 0.07. From this we show that increased scattering observed from SFDI is a reliable analog for measuring the stroke core.

4. Discussion

In this paper we have demonstrated the use of scattering from spatial frequency domain imaging (SFDI) as an optical measure of identifying the stroke core. We first demonstrated the accuracy of OCT signal attenuation in estimating the stroke core by comparing it to the well-established TTC stain. We then compared the spatial overlap between SFDI scattering changes and OCT signal attenuation, following which we compared SFDI to TTC staining. While SFDI has been widely used for various biological and clinical applications (Abookasis et al., 2009; Gioux et al., 2019), it has not been previously used to estimate and follow the progression of the stroke core longitudinally.

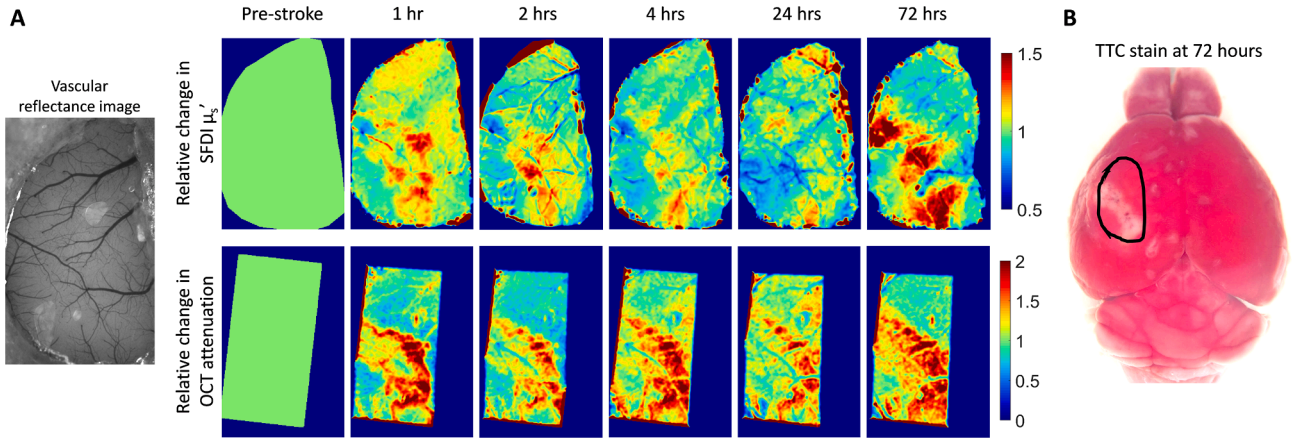

Fig. 5. (A) Percent change in reduced scattering obtain from SFDI (top row) and percent change in OCT signal attenuation (bottom row) from one example mouse at 1 h, 2 h, 4 h, 24 h, and 72 h after stroke. (B) TTC staining at 72 after stoke, black outline indicates cranial window location.

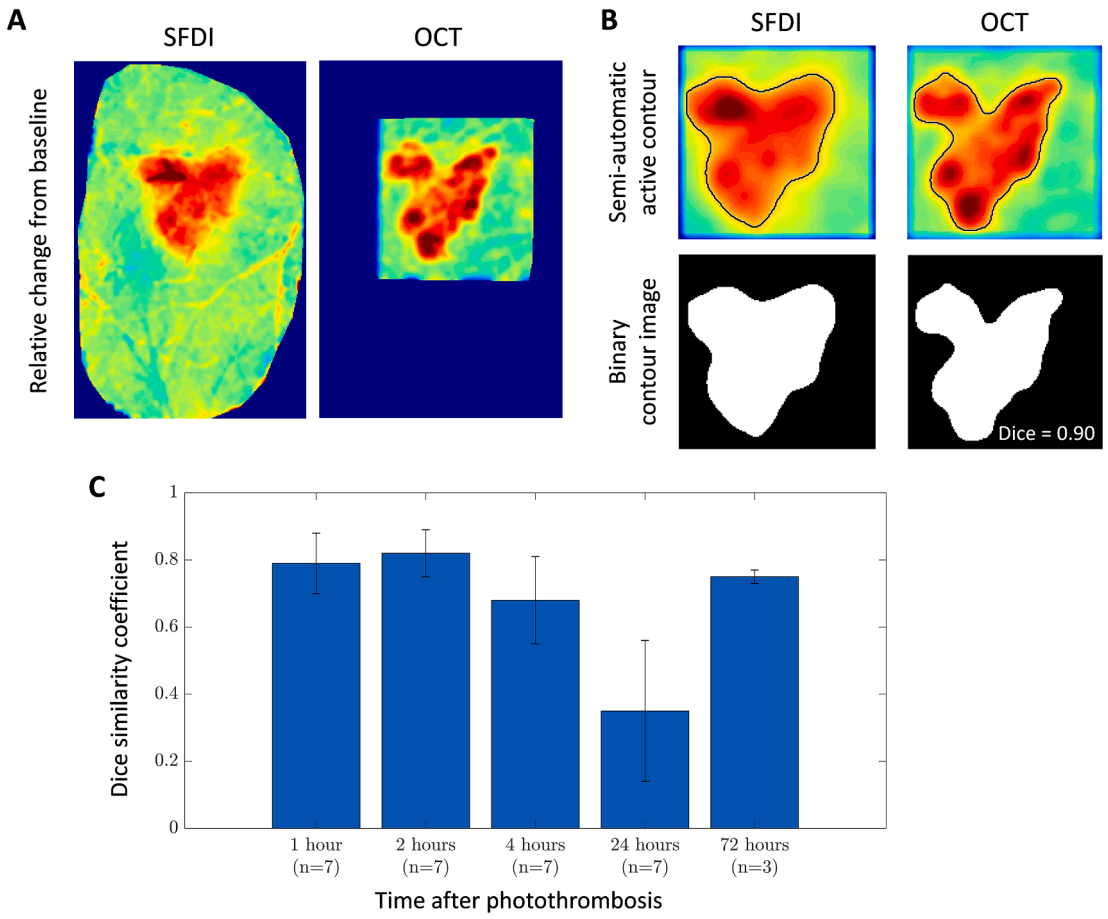

Fig. 6. Dice similarity coefficient workflow and calculation for stroke overlap. (A) Example SFDI and OCT percent change images at 2 h after stroke. (B) Top row: Semi-automatic contour outline of stroke core, bottom row: binary image from contour to calculate the dice similarity coefficient. (C) Dice similarity coefficient for SFDI and OCT stroke core overlap at each time point following stroke represented as mean and standard deviation.

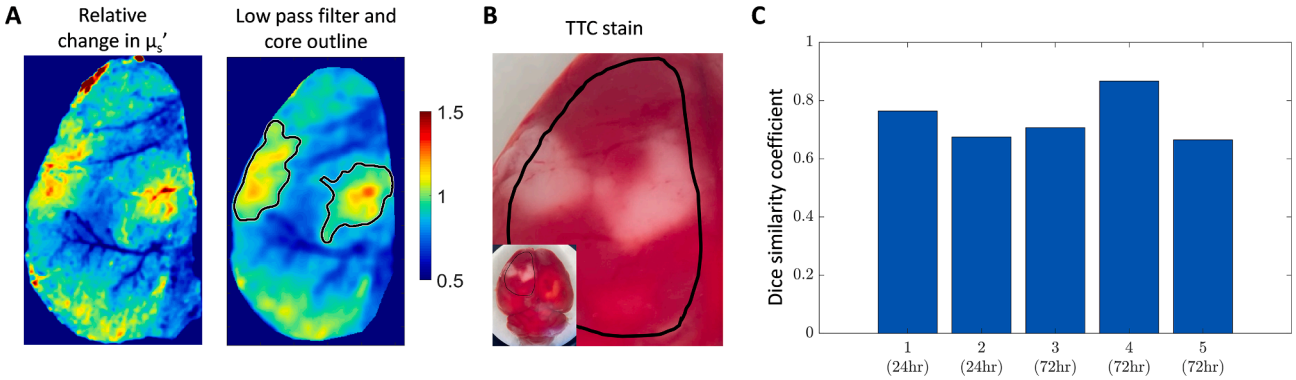

Fig. 7. SFDI spatial overlap with TTC staining. (A) Example percent change image (left) with corresponding low-pass filtered and contoured image (right). (B) TTC stain at the corresponding time point as in (A) (24 h after stroke). (C) Dice similarity coefficient of spatial overlap for five mice.

Following the stroke core is an essential component of monitoring stroke progression in both the acute and chronic phases of stroke recovery. In the acute phase following stroke, DWI in the clinical setting is used to assess the extent of infarct and determine the appropriate treatment protocols, such as the administration of tissue plasminogen activator or clot thrombolysis for recanalization, to prevent the infarct from expanding and also to monitor the effects of such treatments on infarct outcome (Beaulieu et al., 1999; Chatterjee, 2012; Parsons et al., 2002). In the pre-clinical research setting, acute monitoring is valuable to understand the pathophysiological mechanisms that impact tissue outcome and also assess the feasibility of interventions that improve tissue outcome (Erdener et al., 2020; Li et al., 2000). Most of these interventions are targeted towards the penumbra region of the stroke as it is comprised of salvageable tissue that is compromised but not yet dead (Ginsberg, 2008). If left alone, the stroke core expands into the penumbra and results in a larger infarct, but if salvaged the penumbra can

be returned to normal functioning healthy tissue. These studies require monitoring the infarcted tissue at frequent intervals in not only the acute phase but also chronically to truly determine long-term benefits, which require the mouse to not be sacrificed for TTC staining to determine infarct size. In addition to acute studies, longitudinal studies are valuable to understand long-term recovery mechanisms that occur both spontaneously as well as enhanced through rehabilitation (Cramer, 2008b, 2008a). These mechanisms, which primarily occur in the peri-infarct region, are seen as changes to the vascular response to brain activity in fMRI and fNIRS studies (Grefkes and Fink, 2011; Grefkes and Ward, 2014). Apart from observations made in the clinical settings, animal models are used extensively to understand the structural and functional changes that lead to the observed behavioral recovery (Brown et al., 2009; Clarkson et al., 2013; Mostany et al., 2010). This requires longitudinal monitoring from days to weeks and even months, where optical measures of the stroke core could be very useful.

Here, we have validated that OCT and SFDI are reliable optical measures of the stroke core when compared to TTC staining, thereby allowing longitudinal studies. TTC, or triphenyl-tetrazolium chloride, is an indicator used to determine ongoing cellular energy metabolism. Due to its ability to detect tissue viability, by differentiating between metabolically active or inactive tissue, it is used extensively in pre-clinical stroke research to identify damaged tissue and evaluate infarct size due to the stroke (Türeyen et al., 2004). A drawback of TTC staining is that it needs to be performed within 72 h of stroke induction, with 24 h after stroke being the most commonly used time point (Liu et al., 2009). The reason for this is that TTC at later time points is confounded by the robust inflammatory response that results due to stroke and is typical of the secondary or delayed phase of the response to ischemia. This response involves the migration of inflammatory cells towards the stroke core, which play an important role in the post-ischemic recovery period. With the presence of these active cells in the stroke core and peri-infarct region, TTC staining is no longer able to accurately differentiate metabolically dead tissue as these active cells would show viable tissue and mask the true region of inactive tissue. Therefore, TTC staining has to be performed within 72 h after stroke induction, which is before inflammatory cells have established themselves in the stroke affected region, and is therefore a serious limitation when designing long-term experiments. The mechanisms that result from stroke that lead to metabolically dead tissue present themselves as optical changes in tissue properties that can be imaged (Choi et al., 2019; Liang et al., 2007; Srinivasan et al., 2013). We have shown that OCT signal attenuation and SFDI increased scattering at 24 and 72 h after stroke have on average greater than 70% overlap with metabolically dead tissue that was identified with TTC staining. Therefore, by using OCT or SFDI we can capture the spatial extent of the infarct and identify the stroke core and peri-infarct regions while still being able to perform longitudinal stroke experiments.

In addition to imaging at the time points when TTC would have been done, we can use the same imaging techniques to monitor the progression of ischemia throughout the acute phase and sub-acute phase at various time points as the progression can be very dynamic and sometimes biphasic in nature (Uno et al., 2015). In the early hours following stroke it has been hypothesized that cellular and organelle swelling occur due to metabolic dysfunction, which leads to intracellular water accumulation. This presents itself as changes in optical properties of the tissue, which begin as early as 30 min after stroke induction. We have shown changes in optical scattering at 1 h, 2 h, 4 h, 24 h, and 72 h after stroke induction. We observed greater than 70% overlap in the spatial extent of optical changes between OCT and SFDI at all the time points after stroke except 24 h, which showed low overlap and high variability. This was due to the fact that scattering changes were inconsistent in both OCT and SFDI across all animals at 24 h. One explanation for this inconsistency is the effect of reperfusion time on scattering changes and tissue outcome. Evidence has indicated that ischemic hyperintensity seen with DWI in rats can be reversible or biphasic if reperfusion is performed shortly after stroke induction (Li et al., 2000; Minematsu et al., 1992). Our photothrombosis model allows for spontaneous recanalization of the occluded vessel after the 1 h photothrombosis session is complete. While this lends well to study the effect of reperfusion or reflects more naturally what happens in stroke, it introduces variability in the tissue response. The inconsistency seen with tissue scattering at 24 h can be explained when time to reperfusion following occlusion is taken into consideration. Animals that showed reperfusion within 4 h, assessed through laser speckle imaging, showed more inconsistent scattering at 24 h compared to animals that reperfused after 4 h or did not reperfused at all. Reperfusion variability can also increase variability in tissue water content at 24 h, as reperfusion can be associated with an oxidative injury, which can damage the blood brain barrier and lead to vasogenic edema. We speculate that the tissue water content, independent from cellular swelling, may be affecting our results at certain time points. However, the infarct had stabilized at 72 h after stroke and proved to be a better determinant of tissue outcome. Though the point of this paper was not to study the effects of reperfusion time on tissue outcome, we hope to address that question in future experiments.

This approach has a few limitations worth noting. The first is the difference in tissue depth interrogated by OCT and SFDI. Here, we are using a depth of 450 μm in OCT, as larger depths provided more accurate fitting of the data while still remaining within gray matter. Additionally, due to a relatively small and heterogeneous infarct caused by photothrombosis compared to a stronger MCA occlusion, a larger depth provided better visualization of the changing infarct. SFDI on the other hand is integrating across a depth of approximately 300 μm, as calculated from previously published papers (Hayakawa et al., 2018; Lin et al., 2013). We do not expect this difference in integrated tissue volume to have a notable effect on the estimated lateral spatial extent of the stroke core. A second limitation is the crosstalk observed between absorption and scattering in the large blood vessels. Blood is very absorbing at 530 nm, making it challenging to accurately separate scattering from absorption as visualized by its coupling in the LUT. While this can be overcome by using longer wavelengths we advocate for the use of 530 nm for two main reasons, one is that we are interested in mapping scattering changes in the tissue and not the blood vessels, and two, 530 nm is the isosbestic point of hemoglobin therefore allowing estimation of total hemoglobin concentrations, which is beneficial for studies monitoring changes in hemodynamics following stroke. Future studies can address this crosstalk issue by performing a series of phantom measurements in a physiologically relevant range of optical properties across different wavelengths to quantify the accuracy of the SFDI estimates.

In conclusion, we have validated the use of OCT as an optical indicator of the stroke core by computing signal attenuation and comparing against TTC. We have applied the use of SFDI as a mesoscopic measure of spatial changes to optical properties, which was validated against both OCT and TTC. Changes in optical scattering as determined by SFDI is a reliable optical analog of the stroke core thereby allowing longitudinal experiments without the need for sacrificing animals acutely. Additionally, SFDI has the advantage of providing a wide-field approach to detect the stroke core when compared to OCT and traditional histological approaches.

5. Data and code availability statement

The data and code that support the findings of this study are available on GitHub at https://github.com/smrithisunil/StrokeScatteringSFDI.

Disclosures

The authors declare no potential conflicts of interest with respect to the research, authorship, and/or publication of this article.

CRediT authorship contribution statement

Smrithi Sunil: Conceptualization, Methodology, Investigation, Formal analysis, Writing - original draft. **Sefik Evren Erdener:** Conceptualization, Investigation, Formal analysis, Funding acquisition. **Xiaojun Cheng:** Methodology, Software. **Sreekanth Kura:** Software. **Jianbo Tang:** Methodology, Software. **John Jiang:** Methodology. **Kavon Karrobi:** Methodology, Supervision. **Kıvılcım Kılıç:** Methodology, Supervision. **Darren Roblyer:** Conceptualization, Methodology, Supervision. **David A. Boas:** Conceptualization, Methodology, Formal analysis, Supervision, Funding acquisition.

Acknowledgements

This work was supported by the National Institute of Health [R01-EB021018, R01-NS108472, R01-MH111359], and Hacettepe University Scientific Research Projects Coordination Unit [TUI-2019-18106].

References

Abookasis, D., Lay, C.C., Mathews, M.S., Linskey, M.E., Frostig, R.D., Tromberg, B.J., 2009. Imaging cortical absorption, scattering, and hemodynamic response during ischemic stroke using spatially modulated near-infrared illumination. J. Biomed. Opt. 14, 024033 https://doi.org/10.1117/1.3116709.

Applegate, M.B., Karrobi, K., Angelo, J.P., Austin, W.M., Tabassum, S.M., Aguénounon, E., Tilbury, K., Saager, R.B., Gioux, S., Roblyer, D.M., 2020. OpenSFDI: an open-source guide for constructing a spatial frequency domain imaging system. J. Biomed. Opt. 25, 1. https://doi.org/10.1117/1.jbo.25.1.016002.

Ayata, C., Dunn, A.K., Gursoy-Özdemir, Y., Huang, Z., Boas, D.A., Moskowitz, M.A., 2004. Laser speckle flowmetry for the study of cerebrovascular physiology in normal and ischemic mouse cortex. J. Cereb. Blood Flow Metab. 24, 744–755. https://doi.org/10.1097/01.WCB.0000122745.72175.D5.

Bacigaluppi, M., Comi, G., Hermann, D.M., 2010. Animal models of ischemic stroke. Part two: modeling cerebral ischemia. Open Neurol. J. 4, 34–38. https://doi.org/10.2174/1874205X01004020034.

Beaulieu, C., De Crespigny, A., Tong, D.C., Moseley, M.E., Albers, G.W., Marks, M.P., 1999. Longitudinal magnetic resonance imaging study of perfusion and diffusion in stroke: evolution of lesion volume and correlation with clinical outcome. Ann. Neurol. 46, 568–578. https://doi.org/10.1002/1531-8249(199910)46:4<568::AID-ANA4>3.0.CO;2-R.

Blicher, J.U., Stagg, C.J., O'Shea, J., Østergaard, L., MacIntosh, B.J., Johansen-Berg, H., Jezzard, P., Donahue, M.J., 2012. Visualization of altered neurovascular coupling in chronic stroke patients using multimodal functional MRI. J. Cereb. Blood Flow Metab. 32, 2044–2054. https://doi.org/10.1038/jcbfm.2012.105.

Boas, D.A., Dunn, A.K., 2010. Laser speckle contrast imaging in biomedical optics. J. Biomed. Opt. 15, 011109 https://doi.org/10.1117/1.3285504.

Boas, D.A., Culver, J.P., Stott, J.J., Dunn, A.K., 2002. Three dimensional Monte Carlo code for photon migration through complex heterogeneous media including the adult human head. Opt. Express 10, 159. https://doi.org/10.1364/oe.10.000159.

Brendel, M., Kleinberger, G., Probst, F., Jaworska, A., Overhoff, F., Blume, T., Albert, N. L., Carlsen, J., Lindner, S., Gildehaus, F.J., Ozmen, L., Suárez-Calvet, M., Bartenstein, P., Baumann, K., Ewers, M., Herms, J., Haass, C., Rominger, A., 2017. Increase of TREM2 during aging of an Alzheimer's disease mouse model is paralleled by microglial activation and amyloidosis. Front. Aging Neurosci. 9, 1–13. https://doi.org/10.3389/fnagi.2017.00008.

Brown, C.E., Li, P., Boyd, J.D., Delaney, K.R., Murphy, T.H., 2007. Extensive turnover of dendritic spines and vascular remodeling in cortical tissues recovering from stroke. J. Neurosci. 27, 4101–4109. https://doi.org/10.1523/JNEUROSCI.4295-06.2007.

Brown, C.E., Aminoltejari, K., Erb, H., Winship, I.R., Murphy, T.H., 2009. In vivo voltage-sensitive dye imaging in adult mice reveals that somatosensory maps lost to stroke are replaced over weeks by new structural and functional circuits with prolonged modes of activation within both the peri-infarct zone and distant sites. J. Neurosci. 29, 1719–1734. https://doi.org/10.1523/JNEUROSCI.4249-08.2009.

Carmichael, S.T., 2005. Rodent models of focal stroke: Size, mechanism, and purpose. NeuroRX 2, 396–409. https://doi.org/10.1602/neurorx.2.3.396.

Cassidy, J.M., Cramer, S.C., 2017. Spontaneous & therapeutic-induced mechanisms of functional recovery after stroke. Transl. Stroke Res. 8, 33–46. https://doi.org/10.1007/s12975-016-0467-5.Spontaneous.

Chalela, J.A., Kang, D.W., Luby, M., Ezzeddine, M., Latour, L.L., Todd, J.W., Dunn, B., Warach, S., 2004. Early MRI findings in patients receiving tissue plasminogen activator predict outcome: insights into the pathophysiology of acute stroke in the thrombolysis Era. Ann. Neurol. 55, 105–112. https://doi.org/10.1002/ana.10781.

Chatterjee, S., 2012. Recombinant tissue plasminogen activator for acute ischemic stroke. Cardiol. Rev. 28.

Choi, W.J., Li, Y., Wang, R.K., 2019. Monitoring acute stroke progression: multi-parametric OCT imaging of cortical perfusion, flow, and tissue scattering in a mouse model of permanent focal ischemia. IEEE Trans. Med. Imaging 38, 1427–1437. https://doi.org/10.1109/TMI.2019.2895779.

Clarkson, A.N., López-Valdés, H.E., Overman, J.J., Charles, A.C., Brennan, K.C., Thomas Carmichael, S., 2013. Multimodal examination of structural and functional remapping in the mouse photothrombotic stroke model. J. Cereb. Blood Flow Metab. 33, 716–723. https://doi.org/10.1038/jcbfm.2013.7.

Cramer, S.C., 2008a. Repairing the human brain after stroke: I. Mechanisms of spontaneous recovery. Ann. Neurol. 63, 272–287. https://doi.org/10.1002/ana.21393.

Cramer, S.C., 2008b. Repairing the human brain after stroke II. Restorative therapies. Ann. Neurol. 63, 549–560. https://doi.org/10.1002/ana.21412.

Cuccia, D.J., Bevilacqua, F., Durkin, A.J., Ayers, F.R., Tromberg, B.J., 2009. Quantitation and mapping of tissue optical properties using modulated imaging. J. Biomed. Opt. 14, 024012 https://doi.org/10.1117/1.3088140.

Dunn, A.K., 2012. Laser speckle contrast imaging of cerebral blood flow. Ann. Biomed. Eng. 40, 367–377. https://doi.org/10.1007/s10439-011-0469-0.

Dunn, A.K., Bolay, H., Moskowitz, M.A., Boas, D.A., 2001. Dynamic imaging of cerebral blood flow using laser speckle. J. Cereb. Blood Flow Metab. 195–201 https://doi.org/10.1097/00004647-200103000-00002.

Erdener, Ş.E., Tang, J., Sajjadi, A., Kılıç, K., Kura, S., Schaffer, C.B., Boas, D.A., 2017. Spatio-temporal dynamics of cerebral capillary segments with stalling red blood cells. J. Cereb. Blood Flow Metab. https://doi.org/10.1177/0271678X17743877.

Erdener, Ş.E., Tang, J., Kılıç, K., Postnov, D., Giblin, J.T., Kura, S., Chen, I.A., Vayisoğlu, T., Sakadžić, S., Schaffer, C.B., Boas, D.A., 2020. Dynamic capillary stalls in reperfused ischemic penumbra contribute to injury: a hyperacute role for neutrophils in persistent traffic jams. J. Cereb. Blood Flow Metab. https://doi.org/10.1177/0271678X20914179.

Ginsberg, M.D., 2008. Neuroprotection for ischemic stroke: past, present and future. Neuropharmacology 55, 363–389. https://doi.org/10.1016/j.neuropharm.2007.12.007.

Gioux, S., Mazhar, A., Cuccia, D.J., 2019. Spatial frequency domain imaging in 2019: principles, applications, and perspectives. J. Biomed. Opt. 24, 1–18. https://doi.org/10.1117/1.JBO.24.7.071613.

Grefkes, C., Fink, G.R., 2011. Reorganization of cerebral networks after stroke: new insights from neuroimaging with connectivity approaches. Brain 134, 1264–1276. https://doi.org/10.1093/brain/awr033.

Grefkes, C., Ward, N.S., 2014. Cortical reorganization after stroke: how much and how functional? Neuroscientist 20, 56–70. https://doi.org/10.1177/1073858413491147.

Hayakawa, C.K., Karrobi, K., Pera, V., Roblyer, D., Venugopalan, V., 2018. Optical sampling depth in the spatial frequency domain. J. Biomed. Opt. 24, 1. https://doi.org/10.1117/1.jbo.24.7.071603.

Helmchen, F., Denk, W., 2005. Deep tissue two-photon microscopy. Nat. Methods 2, 932–940. https://doi.org/10.1038/nmeth818.

Johansen-berg, H., 2007. Functional imaging of stroke recovery: what have we learnt and where do we go from here? Int. J. Stroke 2, 7–16. https://doi.org/10.1111/j.1747-4949.2007.00093.x.

Johansen-Berg, H., Dawes, H., Guy, C., Smith, S.M., Wade, D.T., Matthews, P.M., 2002. Correlation between motor improvements and altered fMRI activity after rehabilitative therapy. Brain 125, 2731–2742. https://doi.org/10.1093/brain/awf282.

Kim, T.H., Zhang, Y., Lecoq, J., Jung, J.C., Li, J., Zeng, H., Niell, C.M., Schnitzer, M.J., 2016. Long-term optical access to an estimated one million neurons in the live mouse cortex. Cell Rep. 17, 3385–3394. https://doi.org/10.1016/j.celrep.2016.12.004.

Lake, E.M.R., Bazzigaluppi, P., Stefanovic, B., 2016. Functional magnetic resonance imaging in chronic ischaemic stroke. Philos. Trans. R. Soc. B Biol. Sci. 371, 1–11. https://doi.org/10.1098/rstb.2015.0353.

Li, F., Liu, K.F., Silva, M.D., Omae, T., Sotak, C.H., Fenstermacher, J.D., Fisher, M., 2000. Transient and permanent resolution of ischemic lesions on diffusion- weighted imaging after brief periods of focal ischemia in rats: correlation with histopathology. Stroke 31, 946–954. https://doi.org/10.1161/01.STR.31.4.946.

Liang, D., Bhatta, S., Gerzanich, V., Simard, J.M., 2007. Cytotoxic edema: mechanisms of pathological cell swelling. Neurosurg. Focus 22. https://doi.org/10.3171/foc.2007.22.5.3. E2–E2.

Lin, A.J., Ponticorvo, A., Konecky, S.D., Cui, H., Rice, T.B., Choi, B., Durkin, A.J., Tromberg, B.J., 2013. Visible spatial frequency domain imaging with a digital light microprojector. J. Biomed. Opt. 18, 096007 https://doi.org/10.1117/1.JBO.18.9.096007.

Liu, F., Schafer, D.P., McCullough, L.D., 2009. TTC, Fluoro-Jade B and NeuN staining confirm evolving phases of infarction induced by middle cerebral artery occlusion. J. Neurosci. Methods 179, 1–8. https://doi.org/10.1016/j.jneumeth.2008.12.028.

Lo, E.H., 2008. A new penumbra: transitioning from injury into repair after stroke. Nat. Med. 14, 497–500. https://doi.org/10.1038/nm1735.

Lo, E.H., Dalkara, T., Moskowitz, M.A., 2003. Neurological diseases: mechanisms, challenges and opportunities in stroke. Nat. Rev. Neurosci. 4, 399–414. https://doi.org/10.1038/nrn1106.

Meng, X., Fisher, M., Shen, Q., Sotak, C.H., Duong, T.Q., 2004. Characterizing the diffusion/perfusion mismatch in experimental focal cerebral ischemia. Ann. Neurol. 55, 207–212. https://doi.org/10.1002/ana.10803.

Minematsu, K., Li, L., Sotak, C.H., Davis, M.A., Fisher, M., 1992. Reversible focal ischemic injury demonstrated by diffusion-weighted magnetic resonance imaging in rats. Stroke 23, 1304–1310. https://doi.org/10.1161/01.STR.23.9.1304.

Moskowitz, M.A., Lo, E.H., Iadecola, C., 2010. The science of stroke: mechanisms in search of treatments. Neuron 67, 181–198. https://doi.org/10.1016/j.neuron.2010.07.002.

Mostany, R., Chowdhury, T.G., Johnston, D.G., Portonovo, S.A., Carmichael, S.T., Portera-Cailliau, C., 2010. Local hemodynamics dictate long-term dendritic plasticity in peri-infarct cortex. J. Neurosci. 30, 14116–14126. https://doi.org/10.1523/JNEUROSCI.3908-10.2010.

Murphy, T.H., Corbett, D., 2009. Plasticity during stroke recovery: from synapse to behaviour. Nat. Rev. Neurosci. 10, 861–872. https://doi.org/10.1038/nrn2735.
Neumann-haefelin, T., Wenserski, F., Siebler, M., 1999. The DWI / PWI mismatch region in acute stroke. Stroke 1591–1597.
Parsons, M.W., Barber, P.A., Chalk, J., Darby, D.G., Rose, S., Desmond, P.M., Gerraty, R. P., Tress, B.M., Wright, P.M., Donnan, G.A., Davis, S.M., 2002. Diffusion- and perfusion-weighted MRI response to thrombolysis in stroke. Ann. Neurol. 51, 28–37. https://doi.org/10.1002/ana.10067.
Parthasarathy, A.B., Kazmi, S.M.S., Dunn, A.K., 2010. Quantitative imaging of ischemic stroke through thinned skull in mice with Multi Exposure Speckle Imaging. Biomed. Opt. Express 1, 246. https://doi.org/10.1364/boe.1.000246.
AU - Ponticorvo, A., AU - Dunn, A.K., 2010. How to Build a Laser Speckle Contrast Imaging (LSCI) System to Monitor Blood Flow. JoVE e2004. DOI:10.3791/2004.
Schrandt, C.J., Kazmi, S.S., Jones, T.A., Dunn, A.K., 2015. Chronic monitoring of vascular progression after ischemic stroke using multiexposure speckle imaging and two-photon fluorescence microscopy. J. Cereb. Blood Flow Metab. 35, 933–942. https://doi.org/10.1038/jcbfm.2015.26.
Somjen, G.G., 2001. Mechanisms of spreading depression and hypoxic spreading depression-like depolarization. Physiol. Rev. 81, 1065–1096. https://doi.org/10.1152/physrev.2001.81.3.1065.
Srinivasan, V.J., Mandeville, E.T., Can, A., Blasi, F., Climov, M., Daneshmand, A., Lee, J. H., Yu, E., Radhakrishnan, H., Lo, E.H., Sakadžić, S., Eikermann-Haerter, K., Ayata, C., 2013. Multiparametric, longitudinal optical coherence tomography imaging reveals acute injury and chronic recovery in experimental ischemic stroke. PLoS One 8. https://doi.org/10.1371/journal.pone.0071478.
Strong, A.J., Bezzina, E.L., Anderson, P.J.B., Boutelle, M.G., Hopwood, S.E., Dunn, A.K., 2006. Evaluation of laser speckle flowmetry for imaging cortical perfusion in experimental stroke studies: quantitation of perfusion and detection of peri-infarct depolarisations. J. Cereb. Blood Flow Metab. 26, 645–653. https://doi.org/10.1038/sj.jcbfm.9600240.
Sunil, S., Erdener, S.E., Lee, B.S., Postnov, D., Tang, J., Kura, S., Cheng, X., Chen, I.A., Boas, D.A., Kılıç, K., 2020. Awake chronic mouse model of targeted pial vessel occlusion via photothrombosis. Neurophotonics 7, 1–18.
Tabassum, S., Zhao, Y., Istfan, R., Wu, J., Waxman, D.J., Roblyer, D., 2016. Feasibility of spatial frequency domain imaging (SFDI) for optically characterizing a preclinical oncology model. Biomed. Opt. Express 7, 4154. https://doi.org/10.1364/boe.7.004154.
Tang, J., Erdener, S.E., Fu, B., Boas, D.A., 2017. Capillary red blood cell velocimetry by phase-resolved optical coherence tomography. Opt. Lett. 42, 3976–3979. https://doi.org/10.1364/OL.42.003976.
Tang, J., Erdener, S.E., Li, B., Fu, B., Sakadzic, S., Carp, S.A., Lee, J., Boas, D.A., 2018. Shear-induced diffusion of red blood cells measured with dynamic light scattering-optical coherence tomography. J. Biophotonics 11, e201700070. https://doi.org/10.1002/jbio.201700070.
Traystman, R.J., 2003. Animal models of focal and global cerebral ischemia. ILAR J. 44, 85–95. https://doi.org/10.1093/ilar.44.2.85.
Türeyen, K., Vemuganti, R., Sailor, K.A., Dempsey, R.J., 2004. Infarct volume quantification in mouse focal cerebral ischemia: a comparison of triphenyltetrazolium chloride and cresyl violet staining techniques. J. Neurosci. Methods 139, 203–207. https://doi.org/10.1016/j.jneumeth.2004.04.029.
Uno, H., Nagatsuka, K., Kokubo, Y., Higashi, M., Yamada, N., Umesaki, A., Toyoda, K., Naritomi, H., 2015. Detectability of ischemic lesions on diffusion-weighted imaging is biphasic after transient ischemic attack. J. Stroke Cerebrovasc. Dis. 24, 1059–1064. https://doi.org/10.1016/j.jstrokecerebrovasdis.2014.12.037.
Wang, H., Magnain, C., Sakadžić, S., Fischl, B., Boas, D.A., 2017. Characterizing the optical properties of human brain tissue with high numerical aperture optical coherence tomography. Biomed. Opt. Express 8, 5617. https://doi.org/10.1364/BOE.8.005617.
Watson, B.D., Dietrich, W.D., Busto, R., Wachtel, M.S., Ginsberg, M.D., 1985. Induction of reproducible brain infarction by photochemically initiated thrombosis. Ann. Neurol. 17, 497–504. https://doi.org/10.1002/ana.410170513.
Wilson, J.D., Bigelow, C.E., Calkins, D.J., Foster, T.H., 2005. Light scattering from intact cells reports oxidative-stress-induced mitochondrial swelling. Biophys. J. 88, 2929–2938. https://doi.org/10.1529/biophysj.104.054528.
Winship, I.R., Murphy, T.H., 2008. In vivo calcium imaging reveals functional rewiring of single somatosensory neurons after stroke. J. Neurosci. 28, 6592–6606. https://doi.org/10.1523/JNEUROSCI.0622-08.2008.
Wright, P.W., Brier, L.M., Bauer, A.Q., Baxter, G.A., Kraft, A.W., Reisman, M.D., Bice, A. R., Snyder, A.Z., Lee, J.M., Culver, J.P., 2017. Functional connectivity structure of cortical calcium dynamics in anesthetized and awake mice. PLoS One 12, 1–27. https://doi.org/10.1371/journal.pone.0185759.
Yao, X.C., Foust, A., Rector, D.M., Barrowes, B., George, J.S., 2005. Cross-polarized reflected light measurement of fast optical responses associated with neural activation. Biophys. J. 88, 4170–4177. https://doi.org/10.1529/biophysj.104.052506.
Zou, K.H., Warfield, S.K., Bharatha, A., Tempany, C.M.C., Kaus, M.R., Haker, S.J., Wells, W.M., Jolesz, F.A., Kikinis, R., 2004. Statistical validation of image segmentation quality based on a spatial overlap index. Acad. Radiol. 11, 178–189. https://doi.org/10.1016/S1076-6332(03)00671-8.